

# Computational prediction of the binding site of proteinase 3 to the plasma membrane

Eric Hajjar,<sup>1,2</sup> Maja Mihajlovic,<sup>3</sup> Véronique Witko-Sarsat,<sup>4</sup> Themis Lazaridis,<sup>3</sup> and Nathalie Reuter<sup>1\*</sup>

<sup>1</sup>Computational Biology Unit, BCCS, University of Bergen, N-5008 Bergen, Norway

<sup>2</sup>Department of Chemistry, University of Bergen, Allegaten 41, N-5007 Bergen, Norway

<sup>3</sup>Department of Chemistry, The City College of CUNY Convent Avenue, New York, New York 10031

<sup>4</sup>INSERM U845, Centre de Recherche Necker, Université René Descartes Paris 5, Hôpital Necker, 161 Rue de Sèvres, F-75015 Paris, France

## ABSTRACT

Proteinase 3 (PR3) is a neutrophil-derived serine proteinase localized within cytoplasmic granules which can be released upon activation. PR3 is exposed at the neutrophil plasma membrane where it can mediate proinflammatory effects. Moreover, PR3 membrane expression is of special relevance in patients with Wegener's granulomatosis, a systemic vasculitis presenting anticytoplasmic neutrophil autoantibodies (ANCA) against PR3, which can bind to PR3 expressed at the surface of neutrophils and amplify their activation state. Therefore, it is of special relevance to unravel the molecular mechanisms governing its association with the membrane to be able to modulate it. To this end, we performed molecular dynamics (MD) simulations of PR3 with the implicit membrane model IMM1-GC to identify its interfacial binding site (IBS). Both the energies and structures resulting from the MD suggest that PR3 associates strongly with anionic membranes. We observe a unique IBS consisting of five basic (R177, R186A, R186B, K187, R222) and six hydrophobic (F165, F166, F224, L223, F184, W218) amino acids. The basic residues provide the driving force to orient PR3 at the membrane surface, so that the hydrophobic residues can anchor into the hydrocarbon region. Energy decomposition and *in silico* mutations show that only a few residues account for the membrane association. Similar calculations with HNE suggest a different membrane-binding mechanism. Our results agree with previous experimental observations and this work predicts, for the first time, the structural determinants of the binding of PR3 to membranes.

Proteins 2008; 71:1655–1669.  
© 2007 Wiley-Liss, Inc.

**Key words:** PR3; myeloblastin; human neutrophil elastase; neutrophils; inflammation; molecular dynamics simulations; implicit membrane model; IMM1-GC; interfacial binding site.

## INTRODUCTION

Neutrophils are the most abundant type of leukocytes. They are a key component of innate immunity and are able to mediate both anti-infectious and proinflammatory effects.<sup>1,2</sup> During the acute phase of inflammation, they leave the vasculature and migrate toward the site of inflammation where they can kill microorganisms. Proteinase 3 (PR3), human neutrophil elastase (HNE), and cathepsin G (CatG) are highly homologous antibiotic serine proteases of the polymorphonuclear neutrophils (PMN). They are deleterious mediators involved in proteolytic degradation of connective tissues<sup>3</sup> and are associated with several inflammatory diseases such as emphysema,<sup>4</sup> cystic fibrosis, rheumatoid arthritis, and vasculitis.<sup>5</sup> Although these proteases have been for a long time thought to have similar localization, ligand specificity, and function, they might have very different physiologic roles. Specifically, PR3 behaves as a peripheral membrane protein<sup>6</sup> and it has been shown that its membrane expression appears to be a risk factor in chronic inflammatory diseases such as vasculitis or rheumatoid arthritis.<sup>5,7,8</sup> We previously reported a specific association of PR3 to the plasma membrane, stronger than only an ionic interaction.<sup>6</sup> Owen and collaborators argue in favor of a weak charge-dependent mechanism similar for the three proteases.<sup>9</sup> They also show that PR3 enzymatic activity is not inhibited by its inhibitors  $\alpha$ 1-proteinase inhibitor ( $\alpha$ 1-PI, 52 kDa) and elafin (6 kDa) when bound to outer cell surface of PMN, but only by a low-molecular-weight protease

*Abbreviations:* DMPC, dimyristoylphosphatidylcholine; DMPG, dimyristoylphosphatidylglycerol; HNE, human neutrophil elastase; IBS, interfacial binding site  $\alpha$ 1-PI,  $\alpha$ 1-proteinase inhibitor; PR3, proteinase 3.

The Supplementary Material referred to in this article can be found online at <http://www.interscience.wiley.com/jpages/0887-3585/suppmat/>

Grant sponsor: Research Council of Norway [National Program for Research in Functional Genomics in Norway (FUGE)]; Grant sponsor: National Science Foundation; Grant number: MCB-0615552; Grant sponsors: Vaincre La Mucoviscidose, ABCF Mucoviscidose, AMGEN.

\*Correspondence to: Nathalie Reuter, Computational Biology Unit, BCCS, University of Bergen, Thormohlensgt 55, N-5008 Bergen, Norway. E-mail: [nathalie.reuter@cbu.uib.no](mailto:nathalie.reuter@cbu.uib.no)

Received 6 June 2007; Revised 18 September 2007; Accepted 2 October 2007

Published online 12 December 2007 in Wiley InterScience ([www.interscience.wiley.com](http://www.interscience.wiley.com)).

DOI: 10.1002/prot.21853

inhibitor (PMSF). This suggests that  $\alpha$ 1-PI and elafin are not active on membrane PR3 (mPR3) because of steric hindrance. More recently, the group of Aviram showed evidence of a colocalization of PR3, Fc $\gamma$ RIIIb, and p22phox in the membrane, and that PR3 is localized in lipid raft domains.<sup>10,11</sup> They also report that cleavage of neutrophil glycosylphosphatidylinositol (GPI) anchors by PI-PLC reduces mPR3 and Fc $\gamma$ RIIIb, implicating a GPI-protein, possibly Fc $\gamma$ RIIIb, in the attachment of PR3 to the membrane. Hellmark and coworkers showed that CD177 is expressed on the same subset of neutrophils as mPR3 and that their expression on the plasma membrane is increased or decreased in parallel during cell stimulation or spontaneous apoptosis.<sup>12</sup> This was confirmed by Kettritz and coworkers who suggested CD177 (also known as NB1) as a potential membrane receptor for PR3.<sup>13</sup> NB1 is a neutrophil surface receptor and is inserted into the plasma membrane via a GPI-linker. More recently, we have provided evidence that PR3 but not elastase can be externalized and expressed at the surface of neutrophils during apoptosis in the absence of degranulation. We have also observed that PR3 was associated with phospholipid scramblase 1, a myristoylated membrane protein with a translocase activity, present in lipid rafts and involved in the redistribution of membrane lipids during apoptosis. We next observed that apoptosis-induced PR3 membrane expression dramatically decreased macrophage phagocytosis.<sup>14</sup> Taken together, our data strongly suggest a proinflammatory role of membrane PR3 during apoptosis, which goes against the current dogma of the anti-inflammatory role of apoptosis and appears to be a paradox. A better understanding of the molecular mechanisms involved in PR3/membrane interaction will be required in order to modulate and/or inhibit PR3 membrane expression in neutrophils leading to new anti-inflammatory strategies.

In 1999, Goldmann *et al.* investigated the interaction of PR3 with lipid vesicles.<sup>15</sup> They showed that it partially inserts into the hydrophobic region of dimyristoylphosphatidylcholine (DMPC) and dimyristoylphosphatidylglycerol (DMPG) bilayers, thus confirming that PR3 behaves as a peripheral membrane protein. Based solely on the observation of the structure of the enzyme, the authors suggest one hydrophobic region of the enzyme (F166, I217, W218, L223, and F224) as a potential interaction site with the membrane. This has not been confirmed by mutagenesis experiments later on. They observe, surprisingly, that mPR3 inhibition by  $\alpha$ 1-PI is higher than for the soluble enzyme. According to Owen and coworkers, mPR3 is catalytically active against components of the extracellular matrix<sup>9</sup> while Goldmann *et al.* showed that the esterolytic activity of mPR3 (on liposomes) was reduced by 50%. According to this study, the presence of a substrate would not influence the membrane binding.

Although much work has been aimed at unraveling the mechanism by which PR3 binds to the plasma mem-

brane, much remains unknown, especially, the structure–function relationship of the membrane anchorage has not been investigated. The structure of PR3 has been resolved by X-ray in 1996<sup>16</sup> and shows the typical fold of trypsin-like serine proteases; the catalytic triad sits between two  $\beta$ -barrels. No information on its membrane anchorage is revealed by this structure. Although NMR and X-ray are providing increasing amounts of structural information on membrane proteins, their application to peripheral membrane proteins remains challenging.

Theoretical approaches have proven useful in studying structure and functional mechanisms of integral membrane proteins<sup>17–21</sup> and more recently of peripheral membrane proteins.<sup>22–28</sup> The finite difference Poisson–Boltzmann (FDPB) method is a numerical procedure that solves the electrostatic potential around a macromolecule, using the Poisson–Boltzmann equation of classical electrostatics. FDPB and its variant that includes nonpolar contributions (FDPB-SA) have been used to investigate the binding of particular conformations of peptides and proteins to membranes (e.g. Refs. 22, 29–31). Several examples show the close agreement of FDPB predictions with experimental values.<sup>32–34</sup> For example, the orientation of the FYVE domain at the membrane predicted by FDPB matches with the orientation found subsequently by X-ray.<sup>29,35</sup> However, FDPB is computationally demanding and the protein remains rigid during the calculations.

In cases where the membrane interaction site is known, molecular dynamics (MD) simulations using an explicit membrane model can be used, and thus provide an atomic level of detail of the dynamics and function of the protein embedded in (or anchored at) the lipid bilayer. However, the simulation time required is long<sup>36</sup> and in the absence of structural or biophysical data describing the interfacial binding site (IBS) of the protein to the membrane one needs to sample a large number of configurations to be able to identify the region(s) interacting with the membrane; using for example many different starting conformations. Simulations with explicit models or FDPB calculations become then quickly intractable.

Considerable efforts have been delivered to develop implicit models which treat the solvent and membranes in a simple but accurate manner.<sup>37–39</sup> We chose to use the implicit membrane model IMM1-GC because it is computationally efficient, and it accounts for the electrostatic interactions between the charged amino acids of the protein and negatively charged lipid head groups. The model has been shown to accurately describe the binding of both transmembrane and amphipathic peptides to neutral and anionic membranes.<sup>37,40</sup> In addition, it has been recently applied to calculate pH-dependent membrane binding free energy of peptides,<sup>41</sup> the free energy of association of transmembrane helices,<sup>42</sup> the membrane-bound structure of  $\alpha$ -synuclein,<sup>43</sup> and the interaction of a fatty acid binding protein with membranes.<sup>44</sup>

In this study, we use MD simulations of PR3 with an implicit membrane model to identify the IBS of the protease. We assume that the mature enzyme has structural features that allow it to directly interact with membranes, regardless of the presence of partner proteins, in agreement with the work of Arnaout and coworkers.<sup>15</sup> The presence of partners would contribute to bring PR3 to the membrane, stabilize its anchorage, and/or contribute to its function at the plasma membrane.

We first analyzed the sequence and the X-ray structure of PR3 to identify potential post-translational modification sites and cationic and hydrophobic patches. Indeed it is acknowledged that both (i) electrostatic complementarities between cationic regions of proteins and anionic membranes and (ii) membrane insertion of interfacial hydrophobic residues should be an important factor in membrane binding of peripheral proteins.<sup>31</sup> We then performed MD simulations of PR3 with the model IMM1-GC, using three membrane types: 50% anionic, 100% anionic, and neutral. To avoid dependency of our results on the starting point of the simulation, six different initial orientations have been used, so that all parts of the protein surface were presented to the membrane. We report in the results section the structural details of the interaction of PR3 with the three membrane models. We used decomposition of the binding energy to investigate the nature of the contribution of the different amino acids of PR3. Finally, we describe the results of similar simulations with HNE and compare the membrane binding mechanism of both enzymes.

## METHODS

### Sequence and structure analysis

S-acylation, also called palmitoylation, attaches reversibly a palmitate group (16-carbon fatty acid) via thioester linkage to cysteines.<sup>45,46</sup> N-Myristoylation consists in the attachment of a myristoyl group (14-carbon fatty acid chain) via a stable amide linkage to a N-terminal glycine.<sup>47</sup> Prenylation attaches a 15-carbon (farnesyl) or 20-carbon (geranylgeranyl) isoprenoid moiety to a cysteine situated at the fourth last position and part of a CAAX motif.<sup>48–50</sup> We inspected the sequence of PR3 (accession number Q4VB08) for potential post-translational modification sites.

Another usual modification is the attachment of a GPI lipid to the carboxyl terminus ( $\omega$ -site) of the polypeptide after proteolytic cleavage of a C-terminal propeptide.<sup>51</sup> We used *big-PI*, a GPI modification site predictor<sup>51–54</sup> to check the presence of GPI modification sites in PR3.

The presence of basic and hydrophobic clusters was investigated in both the sequence and structure of PR3 by checking the occurrence of Arg and Lys aminoacids on the one hand and Ala, Leu, Ile, Val, Trp, Phe, and Tyr on the other hand. The electrostatic potential was calcu-

lated using Grasp.<sup>55</sup> The images were produced using VMD.<sup>56</sup>

### Implicit membrane model

We used the IMM1 model<sup>37</sup> and its extension IMM1-GC<sup>40</sup> to represent the zwitterionic and anionic membranes, respectively. Briefly, the effective energy of the solute (the protein) is given by

$$W_{\text{IMM1}} = E_{\text{intra}} + \Delta G_{\text{solv}} \quad (1)$$

where  $E_{\text{intra}}$  is the intramolecular energy of the solute given by the CHARMM polar hydrogen force field<sup>57</sup> and  $\Delta G_{\text{solv}}$  its solvation free energy calculated as described in Refs. 37, 40. IMM1 is based on the EEF1 model for water-soluble proteins, which uses a linear distance-dependent dielectric constant, neutralizes the ionic side-chains, and adds a Gaussian solvent exclusion term to the CHARMM 19 energy function.<sup>57</sup>

In IMM1, the membrane is represented as a hydrophobic slab. The solvation parameters change smoothly from aqueous values outside the membrane to values corresponding to a nonpolar solvent inside the membrane. In IMM1-GC, the interactions between the charged bilayer and the charged amino acids of the protein are described following the Gouy–Chapman theory<sup>58</sup> for the diffuse electrical double layer. The effective energy is then

$$W_{\text{IMM1-GC}} = W_{\text{IMM1}} + E_{\text{GC}} \quad (2)$$

The IMM1 and IMM1-GC models are implemented in Charmm<sup>59</sup> (from v. c32a1).

To be able to compare our simulations to the work of Goldmann *et al.*<sup>15</sup> we used three membrane types: 100% anionic, 50% anionic, and neutral membranes. The membrane is perpendicular to the  $z$ -axis. The middle of the bilayer corresponds to the origin of the  $z$ -axis. The thickness of the hydrocarbon core is 23 Å corresponding to DMPC and DMPG lipids. In the case of negatively charged membranes, the plane of smeared charge is positioned 3 Å above the membrane plane ( $z = \pm 14.5$  Å). The area per lipid is set to 70 Å<sup>2</sup>, the valence of the lipids to 1, and the salt concentration to 0.03M.<sup>15</sup>

### MD simulations

#### Initial coordinates

The initial set of coordinates used for the MD simulations was prepared from the X-ray structures of PR3 (PDB ID 1fuj, resolution 2.2 Å<sup>16</sup>) and HNE (PDB ID 1ppf, resolution 1.8 Å<sup>60</sup>). For PR3, we chose to use the protein in a monomeric form, chain A, as chains A–D in the PDB file are extremely similar [root mean square deviation (rmsd): 0.4 Å] with  $B$ -factors of comparable magnitude. PR3 monomer and HNE contain 221 and 228 residues, respectively. The disulfide bridges (both

have four) were set as reported earlier.<sup>61</sup> Finally, the coordinates of the missing hydrogen atoms were determined using HBUILD.<sup>62</sup> The protonation state of the ionizable residues was the standard one corresponding to pH 7.

As a result, the total charge of PR3 and HNE was equal to +2 and +11, respectively. The dimensions along the *x*, *y*, and *z* axes of these prepared structures are 45.5 Å, 44.2 Å, and 37.0 Å for PR3 and 47 Å, 43.5 Å, and 37.4 Å for HNE.

### Initial orientation

PR3 and HNE are globular proteins. Their IBS is a priori unknown, and we needed to initiate our simulations with all possible regions of the protein facing the membrane to prevent dependency of our results on the initial conformation. Six different initial orientations were used for each enzyme, each corresponding to a face of a cube containing PR3 (or HNE). Each of the six simulations starts with a different face of the cube toward the membrane plane (cf. Fig. 1). For each orientation, the protein was translated along the *z*-axis so that the corresponding face of the cube was sidelong to the membrane plane. The six corresponding sets of coordinates were saved and will be referred to as the starting structures of the MD simulations.

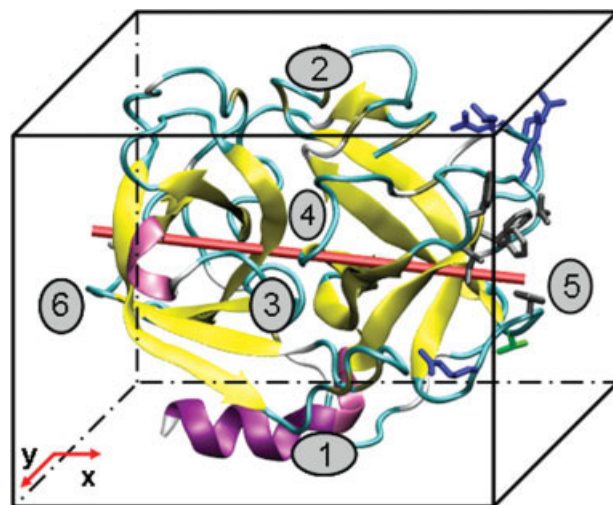


**Figure 1**

Input structures for MD simulations: six different orientations of PR3. The secondary structure elements of PR3 are displayed using cartoons (purple: helices, cyan: loops, yellow: extended sheets). The principal axis of inertia is represented by a red bar. The amino acids of the BC and HC are displayed in sticks and colored by type (grey: hydrophobic, blue: basic, green: polar). The number on each face of the cube corresponds to the simulations labeling and shows the region of PR3 facing the membrane surface in the initial conformation. All orientations can be described as rotations of orientation 1 around *x* or *y*: 2 (180°, *x*), 3 (90°, *x*), 4 (270°, *x*), 5 (90°, *y*), 6 (270°, *y*). [Color figure can be viewed in the online issue, which is available at [www.interscience.wiley.com](http://www.interscience.wiley.com).]

### Simulation procedure

The MD simulations were performed using Charmm (v. c32a1).<sup>59</sup> The energy was briefly minimized, and the systems were then brought to 300 K using periodic reassignment of the velocities to control the temperature. All MD runs were performed for 1000 ps, except the ones starting with orientation 5, which needed 2000 ps in order to achieve energy and structure convergence. For each of the six starting orientations and for each of the three membrane types, the simulations were repeated three times with different initial velocities (seeds randomly chosen). The conformations were stored every picosecond. For each stored conformation we calculated the effective energy of the enzyme in water, using the EEF1.1 force field.<sup>37</sup> The binding energy of PR3 (and HNE) to membranes could thus be calculated every picosecond as the difference between the effective energy with the membrane model IMM1(-GC) and the effective energy in water (EEF1.1):

$$\Delta W_{\text{IMM1-GC}} = \Delta E_{\text{intra}} + \Delta \Delta G_{\text{solv}} + E_{\text{GC}} \quad (3)$$

The same conformation is used to calculate *W* with the membrane model and in water. Both the binding energy and the protein orientation were stable during the last 500 ps of the simulations; this window was chosen as the sampling time.

### Trajectory selection

For each of the three membrane types, six different starting structures of PR3 are used and, for each of these, three simulations are run with different initial velocities. We thus ran 54 simulations in total; 18 for each membrane type and select three for further analysis. In the case of the anionic membranes, all the simulations show a similar anchorage of PR3 to the bilayer. For each membrane type, we select the simulation yielding the lowest effective energy (*W*) and analyze it further. In the case of the zwitterionic membrane, only one starting orientation (orientation 6, all three seeds) leads to an anchorage of PR3; among these three simulations, we select the one leading to the lowest *W*.

### Trajectory analysis

Unless stated otherwise, all analyses were performed using Charmm on the sampling time of the selected simulations.

### PR3 fold

The rmsd between conformations stored during the sampling and the starting structures were calculated using the backbone atoms of PR3 (N, C $\alpha$ , C, O atoms). The average values are 2.53, 2.37, and 2.88 Å for the simulation in 100% anionic, 50% anionic, and zwitterionic membranes, respectively. This is in the same range as the

value obtained when simulating PR3 with implicit water (2.72 Å).

### Energy decomposition

The total binding energy of PR3 can be decomposed into terms that represent the contribution of each type of atom to the change in solvation energy plus the electrostatics term:

$$\Delta W_{\text{IMM1-GC}} = \Delta E_{\text{elec}} + \Delta W_{\text{aromatic}} + \Delta W_{\text{aliphatic}} + \Delta W_{\text{polar}} + E_{\text{GC}} \quad (4)$$

$\Delta E_{\text{elec}}$  is the change in the intramolecular coulombic term when transferring the protein from water to the membrane. Indeed, since the same trajectory is used to calculate  $W(\text{water})$  and  $W(\text{membrane})$ , the bonded terms and the van der Waals contribution cancel out. The next three terms represent the contribution to  $\Delta \Delta G_{\text{solv}}$  [Eq. (3)];  $\Delta W_{\text{aromatic}}$  is the contribution from the aromatic groups (atoms of type CR\* in Charmm19),  $\Delta W_{\text{aliphatic}}$  is the contribution from aliphatic groups (CH\* atom types in Charmm 19) and  $\Delta W_{\text{polar}}$  is the contribution from the polar groups.

The five terms were calculated for each conformation collected during the sampling time of each of the three selected simulations.

### Calculation of the contribution of individual residues

The contributions of each atom of the protein to the solvation free energy are calculated for the average structure of each selected simulation (*eef1 print*). The  $E_{\text{GC}}$  term for residue  $i$  is calculated by extinguishing the charges of all other charged amino acids (K, R, D, E, Nter, Cter) and calculating  $E_{\text{GC}}$  as described earlier. We then calculated the difference with the corresponding terms in water to evaluate the contribution of each atom to the membrane binding energy. The atomic contributions were summed to obtain residue contribution.

### Structure prediction of rat and mouse PR3

The three-dimensional models of the mouse PR3 and NE were built with the program Modeller,<sup>63</sup> using as templates the three-dimensional structure of the human PR3 (PDB ID 1fuj). We also built the model of rat PR3. Because of its extremely high similarity with the mouse variant, our investigation focuses on the latter.

## RESULTS

### Sequence and structure analysis

#### Absence of post-translational modification sites

The reversible binding of proteins to membrane surfaces is often promoted by post-translation linkages such

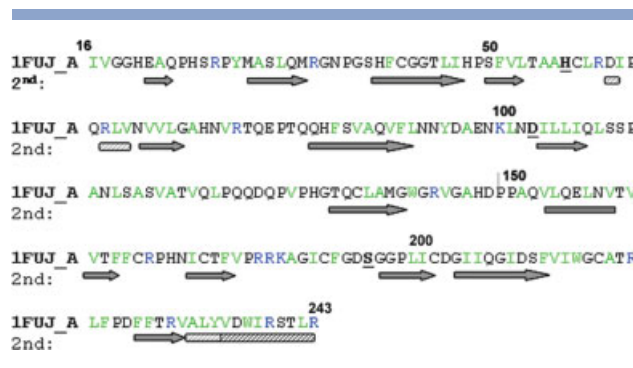


**Figure 2**

Amino acid sequence of the mature PR3 protein. Amino acids are reported in their one-letter code. PR3-chymotrypsin numbering convention is used. Secondary structure elements are reported below the aa sequence: plain grey arrows for extended sheets and dashed rectangles for helices (light grey and black for 3–10 and  $\alpha$ -helices, respectively). The color informs on the nature of the residues: “green” denotes the hydrophobic residues (A, L, I, V, W, F, Y) and “blue” denotes the basic (R and K) residues. [Color figure can be viewed in the online issue, which is available at [www.interscience.wiley.com](http://www.interscience.wiley.com).]

as S-acylation, myristoylation, prenylation, or GPI-linkage on specific aminoacids of the protein sequences.

We inspected the amino acid sequence of PR3 (cf. Fig. 2) to check for the existence of such post-translational modification sites. We found that PR3 cannot be myristoylated as it does not present the N-terminal Met-Gly required motif. It does not present a CAAX box at its C-terminal part and therefore cannot be prenylated. Similarly S-acylation cannot occur on PR3 since its eight cysteines form four disulfide bonds.<sup>16</sup> We could not find any GPI modification sites in PR3.

#### Clusters of basic and hydrophobic amino acids

The sequence of the mature PR3 consists of 221 amino acids and has a total net charge of +2.<sup>61</sup> On Figure 2 we highlighted the hydrophobic and basic amino acids as well as the secondary structure elements of PR3. We observe that the largest cationic “stretch” (residues contiguous in the sequence) is only three-residue long; RRR at position 186A, 186B, and 187. There are numerous residues with a hydrophobic character spread along the sequence of PR3. Interestingly, some regions do combine stretches of basic and hydrophobic residues like <sup>27</sup>RPYMASLQMR<sup>38</sup>, <sup>58</sup>CLRDPQRLV<sup>64</sup>, <sup>165</sup>FFCRPHNICTFVPRRK<sup>187</sup>, or <sup>227</sup>FFTRVALYVDWIRSTLR<sup>243</sup>. The available examples of peripheral proteins show that their net charge can be highly positive (up to +10), neutral, or even highly negative (−13).<sup>31</sup>

More than the net charge, the way the charges are distributed over the surface of a peripheral protein and its electrostatic potential affect its membrane binding. It is therefore necessary to scrutinize the structure of PR3. Figure 3(A) shows the structure of PR3 and its electrostatic potential calculated using GRASP. We observe seven elec-

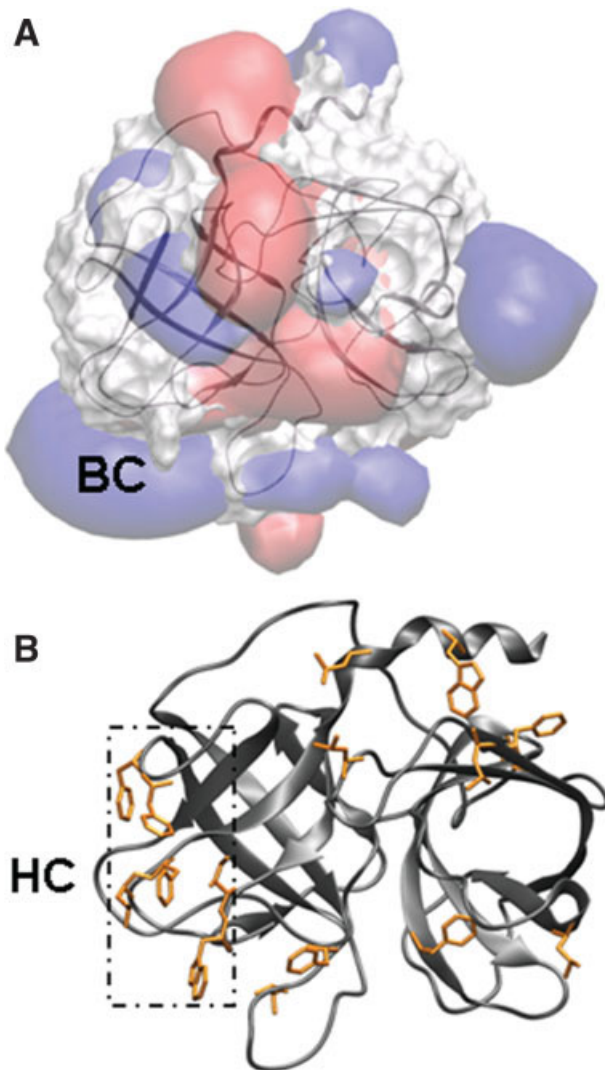


**Figure 3**

Basic and hydrophobic clusters at the surface of PR3. (A) Electrostatic potential of PR3. The equipotential contours calculated using GRASP (cf. Methods section) are colored in blue (+1 kT) and red (-1 kT). We also represent the molecular surface of PR3 on which the electrostatic potential is mapped (blue: positive, red: negative, white: neutral) (B) Amino acids having a solvent accessible surface area greater than 50 Å<sup>2</sup> are represented in orange sticks using a similar orientation of PR3 as in (A). The secondary structural elements are displayed using cartoons. [Color figure can be viewed in the online issue, which is available at [www.interscience.wiley.com](http://www.interscience.wiley.com).]

tropositive regions (blue contours) in the enzyme, the largest one corresponds to <sup>177</sup>RPHNICTFVPRRK<sup>187</sup>. This basic cluster (BC) corresponds to two solvent-exposed loops. The first loop is the <sup>177</sup>RPH<sup>179</sup> motif, <sup>180</sup>NICTFV<sup>185</sup> is then located in a  $\beta$  strand, and <sup>186A</sup>RRK<sup>187</sup> is the second exposed loop. Interestingly, other basic residues (R222, R177) located further in the sequence are structurally close enough to contribute to form a larger cluster.

Figure 3(B) highlights the distribution of the hydrophobic residues on the surface of PR3. The main hydro-

phobic cluster (HC) consists of four solvent exposed loops containing the residues F165, F166, I217, W218, L223, and F224. Interestingly, the identified BC and HC regions are neighboring regions and look like a convenient binding motif; HC sitting in the middle of the described BC. In what follows, this region will be referred to as the putative IBS of PR3.

### MD simulations with IMM1

MD simulations were run as described in the Methods section, using six different starting structures; each one corresponding to a different orientation of PR3 with respect to the membrane plane (cf. Fig. 1 and Methods section).

### Orientations of mPR3 and effective energy

We report in Table I for the six initial orientations and the two anionic membrane types, the distance ( $d$ ) between the center of mass of PR3 and the membrane upper plane, the angle between the principal axis of inertia and the bilayer normal ( $\Theta$ ), and the average of the effective energy of PR3 along the selected simulations ( $W_{\text{IMM1-GC}}$ ; cf. Methods section).

**100% anionic membrane.** The average effective energies ( $W_{\text{IMM1-GC}}$ ) of PR3 at the membrane are of the same range for the six simulations. The binding energies are all negative (supplementary material) meaning that the binding of PR3 to the 100% anionic membrane is favorable. The final orientation of the protein is found to be very similar for the six simulations. Indeed we observe that after rather quick reorientations of the starting structure PR3 adopts a position where the putative IBS is facing the membrane. For example, along simulation 4, the angle between the principal axis of inertia of the protein and the bilayer normal decreases from 84° ( $\Theta_{\text{ini}}$ ) to 8.5° ( $\Theta_{\text{end}}$ ). This is illustrated by the snapshots in Figure 4. The six simulations lead to values of  $\Theta_{\text{end}}$  between 8.5° and 40.8°. Simulation 4 is selected for further analysis, as it is the one yielding the lowest effective energy (-4415.57 kcal/mol) and is thus the optimal conformation of PR3 at the membrane. The corresponding average binding energy is very favorable; -10.87 kcal/mol. The protein effectively anchors to the membrane.

**50% anionic membrane.** Simulation 6 yields the most favorable effective energy (-4408.59 kcal/mol) (cf. Table I) and is selected for further analysis. The corresponding binding energy is -9.04 kcal/mol. Here again we find that the six final orientations are very similar with values of  $\Theta_{\text{end}}$  between 16.7° and 37.4° (30.3° for simulation 6). The orientation and the significant insertion of PR3 to the 50% anionic membrane are very similar to the ones observed for the 100% anionic model.

**Zwitterionic membrane.** The binding of PR3 to the membrane is significantly diminished. Indeed, the protein

**Table I**

Binding Energies of PR3 on the Anionic Membranes

	$\Theta_{\text{ini}}$	100% Anionic			50% Anionic		
		$W_{\text{IMM1-GC}}$	$\Theta_{\text{end}}$	$d$	$W_{\text{IMM1-GC}}$	$\Theta_{\text{end}}$	$d$
Simulation 1	90	$-4391.52 \pm 1.21$	31.2	24.3	$-4385.15 \pm 1.15$	37.4	22.5
Simulation 2	90	$-4392.73 \pm 1.09$	17.6	31.3	$-4390.95 \pm 1.09$	26.6	22.4
Simulation 3	84	$-4397.80 \pm 1.29$	40.8	28.5	$-4402.85 \pm 1.16$	22.6	28.5
Simulation 4	84	$-4415.57 \pm 1.14$	8.5	23.7	$-4399.72 \pm 1.23$	16.7	23.9
Simulation 5	173.6	$-4394.19 \pm 1.17$	33.9	27.1	$-4405.95 \pm 1.13$	28.1	28.3
Simulation 6	6.4	$-4389.87 \pm 1.46$	17.9	23.7	$-4408.59 \pm 1.08$	30.3	21.9

$W_{\text{IMM1-GC}}$ : effective energies of PR3 at the membrane (averages over the sampling time and standard deviation of the mean, in kcal/mol),  $\Theta_{\text{ini}}$  and  $\Theta_{\text{end}}$ : angles (in degrees) between the principal axis of inertia of PR3 and the bilayer normal at the first and the last step of the simulations, respectively;  $d$ : distance (in Å) between the center of mass of PR3 and the membrane plane at the last step of the simulations (the initial value of  $d$  is 21.5 Å, cf. Methods section). For each starting orientation, three simulations were run (using a different seed, cf. Methods section); we report here results from the one leading the lowest  $W$  for each orientation.

moves away from the membrane in all simulations except simulation 6. In the latter the simulation is initiated with PR3 presenting its putative IBS to the membrane interface ( $\Theta_{\text{ini}} = 6.4^\circ$ ). This simulation yields an effective energy of  $-4394.31$  kcal/mol and is selected for further analysis. The corresponding binding energy is  $-3.07$  kcal/mol. It is less favorable than the ones obtained with anionic membranes but still indicates some binding of PR3 to the neutral membrane model.

In what follows, we will present the analysis of only the three selected trajectories (cf. Methods section); simulations 4, 6 and 6 for the 100% anionic, 50% anionic and neutral membrane models, respectively.

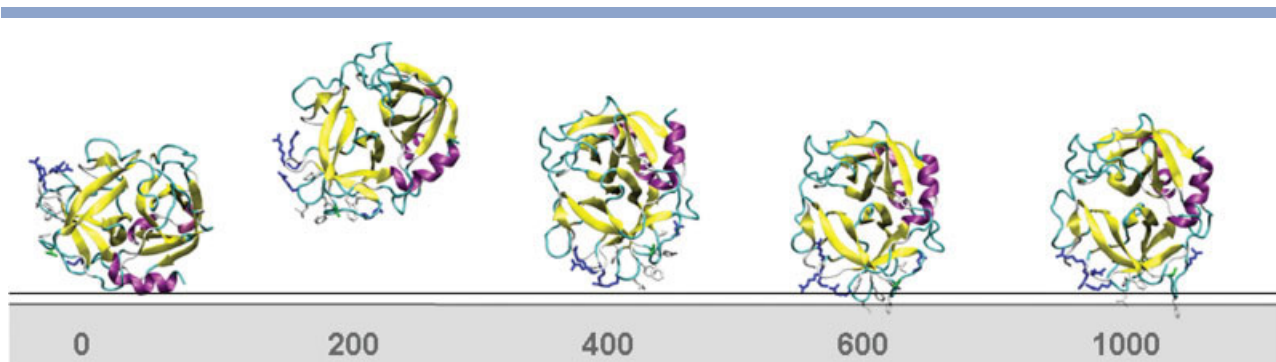
#### Structural details of the interaction with the membrane

As described in the previous section, regardless of its initial orientation, PR3 reorients to present the putative IBS to the membrane model surface if the membrane

carries a negative charge. The same orientation binds favorably to the zwitterionic membrane model although the interaction energy is lower than for the anionic membranes. All three structures are presented on Figure 5.

We observe that PR3 not only interacts favorably but also inserts into the membrane region. Its center of mass (CoM) is positioned at 23.1, 22.4, and 22.6 Å from the hydrocarbon plane of the membrane of the 100% anionic, 50% anionic and zwitterionic membranes, respectively. The position of the CoM with the three membrane models thus reflects an anchoring of the protein. This is illustrated on Figure 5, where the IBS is identified as being composed of four neighboring loops.

The same residues of PR3 seem to be involved in the interaction with the three membrane types. Among them are five basic residues (R177, R186A, R186B, K187, and R222) belonging to the BC identified in the sequence (cf. Sequence and Structure Analysis section). Interestingly, several hydrophobic residues are either contacting or

**Figure 4**

Snapshots of PR3 along simulation 4 with the 100% anionic membrane. Configurations at  $t = 0, 200, 400, 600,$  and  $1000$  ps are displayed using the same representation as on Figure 1. Initially ( $t = 0$ ), PR3 is placed with the C-terminal helix contacting the membrane. At  $t = 200$  ps PR3 has already been moving away from the membrane and starts rotating to present its IBS to the polar heads ( $t = 400$  ps). By  $t = 600$  ps, the hydrophobic residues have inserted into the membrane model while the basic groups are positioned at the interface. The orientation of the enzyme remains the same until the end of the simulation ( $t = 1000$  ps). [Color figure can be viewed in the online issue, which is available at [www.interscience.wiley.com](http://www.interscience.wiley.com).]

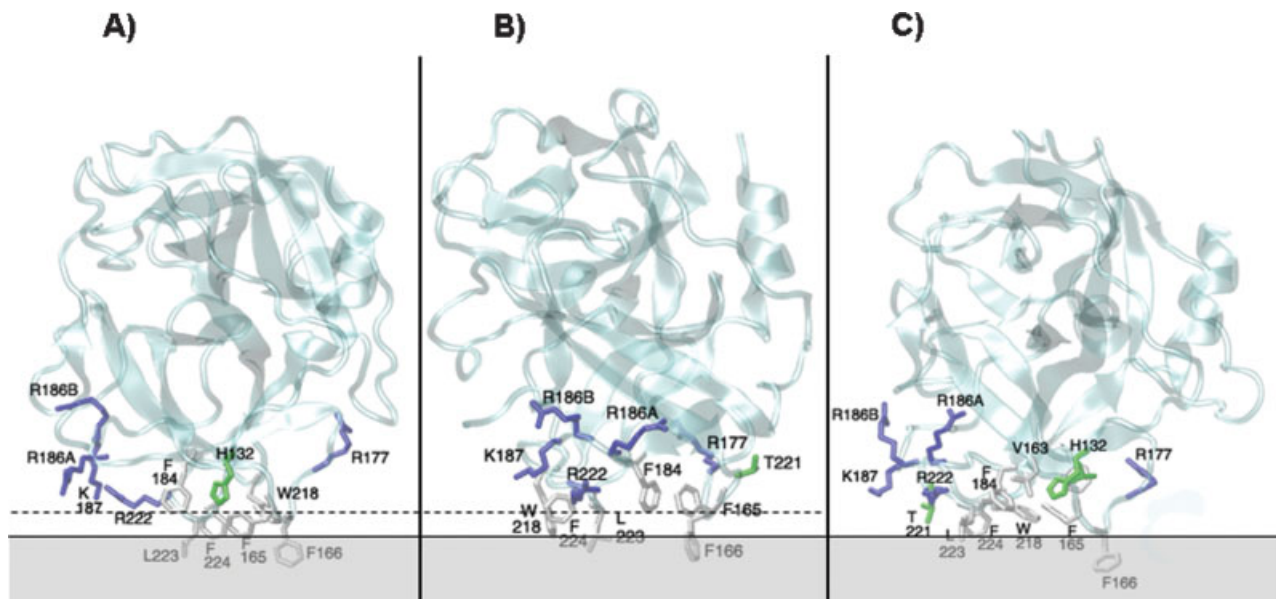


**Figure 5**

Structure of PR3 in 100% anionic (A), 50% anionic (B), and zwitterionic membrane (C). Minimized average structures obtained from the sampling time of each of the three selected simulations. The plane of smeared charge of the membrane model is displayed as a dashed line while a continuous line is used for the upper limit of the hydrophobic region. The secondary structure elements of PR3 are displayed with cartoons. The key residues (R177, R186A, R186B, K187, R222, F165, F166, F184, F224, L223, W218, H132, and T221) are displayed using licorice and colored according to their nature (blue: positively charged, green: polar, light grey: hydrophobic). [Color figure can be viewed in the online issue, which is available at [www.interscience.wiley.com](http://www.interscience.wiley.com).]

inserted into the hydrophobic region of the membrane models: F165, F166, F184, L223, and F224. The polar and hydrophobic residues W218, H132, and T221 are also disposed at the surface of the membrane in an interfacial position.

We superimposed the backbone of the three averaged structures displayed in Figure 5 and calculated the rmsds between the conformation of the zwitterionic and 50% anionic membrane compared to the 100% anionic membrane. Overall the three structures are similar with some local differences. We calculated the rsm on the same alignment for, on one hand, the amino acids folded in beta barrel or helices and, on the other hand, residues located in loops. The rmsd is lower for the helices and sheets (1.69 Å, 1.53 Å for 50% anionic and zwitterionic membrane, respectively) than for the loops (3.3 Å and 3.7 Å, for 50% and zwitterionic membrane, respectively). The main differences are located in the loops carrying the residues of the IBS. This can be seen on Figure 5(C) for example, where R186A and K187 point away from the zwitterionic membrane while they are closer to the plane of smeared charge of the 100% anionic membrane.

### Components of the binding energy

The binding energy of PR3 to membrane ( $\langle \Delta W_{\text{total}} \rangle$ ) can be decomposed into terms that account for the different contributions:  $\Delta W_{\text{aliphatic}}$ ,  $\Delta W_{\text{aromatic}}$ ,  $\Delta W_{\text{polar}}$ ,

$\Delta E_{\text{elec}}$  and  $E_{\text{GC}}$ . The latter accounts for the interactions between the charged residues and the membrane plane containing the anionic polar heads. The averages of each of these five terms were calculated along the sampling time of the MD simulations and are reported in Table II.

The magnitude of the term  $\langle E_{\text{GC}} \rangle$  is seen to increase with the concentration of anionic lipids in the membranes from 6.59 kcal/mol in the 50% anionic membrane to 8.75 kcal/mol in the 100% anionic membrane. This reflects the favorable electrostatic interactions between the basic residues of the IBS of PR3 and the negatively charged membranes. The sum of  $\Delta W_{\text{aliphatic}}$  and  $\Delta W_{\text{aromatic}}$  is favorable and larger in absolute value than the unfavorable contribution from polar groups and electrostatics ( $\Delta W_{\text{polar}} + \Delta E_{\text{elec}}$ ). This is true for the three membranes regardless of their anionic composition. In the extreme case of a neutral membrane the hydrophobic term is the only one favoring the binding of PR3 to the membrane. This is explained by the interaction of hydrophobic residues of PR3 (HC) with the hydrophobic core of the model membranes.

We then investigated the contribution of each residue of PR3 to  $E_{\text{GC}}$  and to the sum of  $\Delta W_{\text{aliphatic}}$ ,  $\Delta W_{\text{aromatic}}$ , and  $\Delta W_{\text{polar}}$ . The calculation is performed on the three average structures of the selected simulations; the results are plotted in Figure 6. The contributions to the  $E_{\text{GC}}$  term are qualitatively similar for both anionic bilayers; for the sake of clarity, we thus chose to plot it in the

**Table II**

Components of the Binding Energies

	100% Anionic	50% Anionic	Zwitterionic
$\langle \Delta W_{\text{total}} \rangle$	$-10.87 \pm 1.61$	$-9.04 \pm 1.53$	$-3.07 \pm 1.63$
$\langle E_{\text{GC}} \rangle$	$-8.75 \pm 0.05$	$-6.59 \pm 0.05$	—
$\langle \Delta W_{\text{polar}} \rangle + \langle \Delta E_{\text{elec}} \rangle$	$6.39 \pm 1.59$	$5.80 \pm 1.75$	$4.61 \pm 1.55$
$\langle \Delta W_{\text{arom.}} \rangle + \langle \Delta W_{\text{aliph.}} \rangle$	$-8.39 \pm 0.13$	$-8.13 \pm 0.12$	$-7.63 \pm 0.11$

Average values over the sampling time and standard deviations of the mean of the different energy terms (in kcal/mol). Only results from the selected simulations are reported.

case of the 100% anionic membrane. Values for amino acids having a negligible contribution are not plotted.

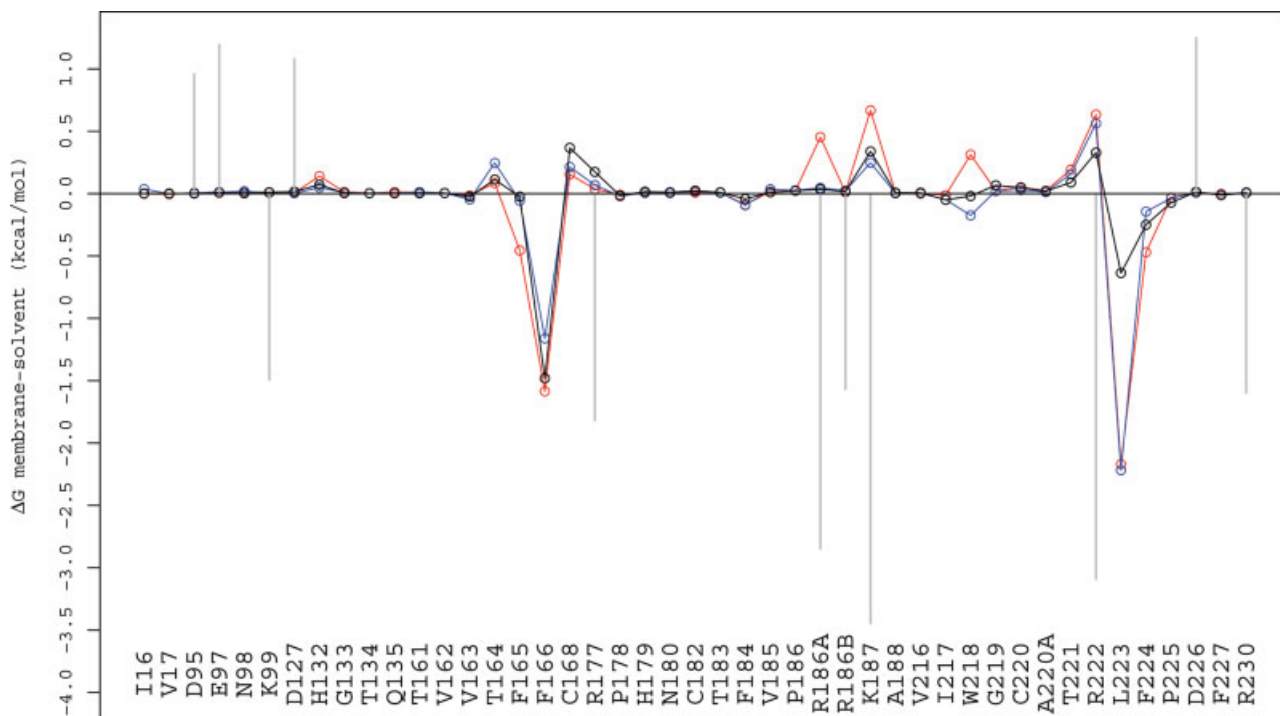
Interestingly, only a few have a significant contribution. This is true for all three membrane types. The positive values correspond to amino acids T164, C168, R177, R186A, K187, W218, T221, and R222. They all are polar residues which are solvent exposed and located close to the membrane plane. This explains their unfavorable contribution when transferring them from water to the membrane. In the case of the anionic membranes, these unfavorable contributions are largely compensated by the GC term of the basic amino acids R177, R186A,

K187, and R222, as well as, for all membrane types, by the contributions of the nonpolar residues F165, F166, L223, and F224. F166 and L223 contribute by up to  $-1.59$  and  $-2.22$  kcal/mol, respectively.

These results indicate that PR3 associates to biological membranes via interactions with basic residues (mainly R186A, R186B, K187, R222) and hydrophobic residues (mainly F166, F165, L223, F224). The former (long range electrostatics) would drive PR3 towards the membrane so that the latter can insert into the hydrophobic core.

### Comparison with the homologous HNE

We simulated HNE following the same procedure as for PR3; we started from six different orientations equivalent to the ones used for PR3 and used the same three membrane types (100%, 50%, and 0% anionic membranes). In the case of a zwitterionic membrane, HNE is consistently driven away from the membrane. It is not the case for the anionic membranes where the binding energies are all negative. However, unlike PR3, HNE does not reorient to present a binding site similar for all initial orientations. In addition no interfacial insertion of HNE is observed except for simulation 6. Simulation 6 is the one yielding the lowest effective energy of HNE for the

**Figure 6**

Amino acids contribution to the terms of the binding energy. The calculation is made on the average structure of PR3 of the selected simulation. The sum of  $\Delta W_{\text{aliphatic}} + \Delta W_{\text{aromatic}} + \Delta W_{\text{polar}}$  for each residue is plotted in red, blue, and black for the 100% anionic, 50% anionic, and zwitterionic membranes, respectively. Grey lines correspond to the GC term for the 100% anionic membrane. The GC term is nonzero only for charged residues (R, K, D, and E). The atomic components were summed for each residue, and only the residues having a contribution greater than 0.05 kcal/mol (absolute value) are reported.

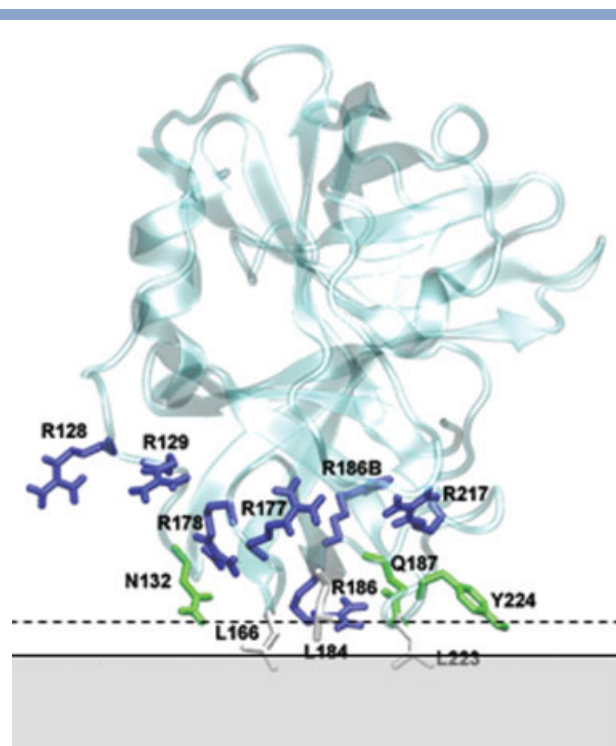


**Figure 7**

Simulation of HNE with a 50% anionic membrane model: average structure. Minimized averaged structure along the sampling time of simulation 6 (see Fig. 5 for legend). [Color figure can be viewed in the online issue, which is available at [www.interscience.wiley.com](http://www.interscience.wiley.com).]

100% and the 50% anionic membranes ( $-18.52$  and  $-12.65$  kcal/mol, respectively) and is thus selected for further analysis. The membrane interaction site of HNE is different from the one found for PR3 (Fig. 7). It contains more basic amino acids and in particular seven arginines R128, R129, R177, R178, R186, R186B, and R217. There are fewer hydrophobic residues than in the IBS of PR3, no phenylalanines or tryptophanes and only L166 and L223 insert into the membrane while L184 seem to remain at the interface. Three polar residues are positioned at the membrane interface: N132, Q187, and Y224.

The binding energy of HNE with anionic membranes has been divided into the same components as for PR3. The sum of the hydrophobic and aromatic terms is  $-6.29$  and  $-3.65$  kcal/mol in the 100% and the 50% anionic membranes, respectively. This term almost cancels out with the term accounting for the sum of the polar and electrostatic contributions,  $7.49$  and  $3.29$  kcal/mol in the 100% and the 50% anionic membranes, respectively. Most of the binding energy of HNE to anionic membranes is explained by the  $E_{GC}$  term,  $-19.67$  and  $-11.82$  kcal/mol in the 100% and the 50% anionic membranes, respectively. This is expected from the proximity of the seven arginines with the membrane surface. In addition, a large portion of the surface of HNE is electropositive

(cf. Fig. 1 in Supplementary Material), unlike PR3, and the basic amino acids are evenly distributed.

### Comparison with the model structure of mouse PR3

The alignment of the human and mouse forms of PR3 [Fig. 8(A)] shows that the amino acids constituting the putative IBS in human PR3 are not all conserved in the murine enzymes. The following substitutions affect the IBS: F166L, F184L, K187A, W218R, R222L, L223Q. The electrostatic potential [Fig. 8(B)] of mouse PR3 is more electronegative than the one of its human form, which might cause a lower affinity for anionic membranes.

## DISCUSSION

Using MD simulations with an implicit membrane model, we investigated for the first time the structural

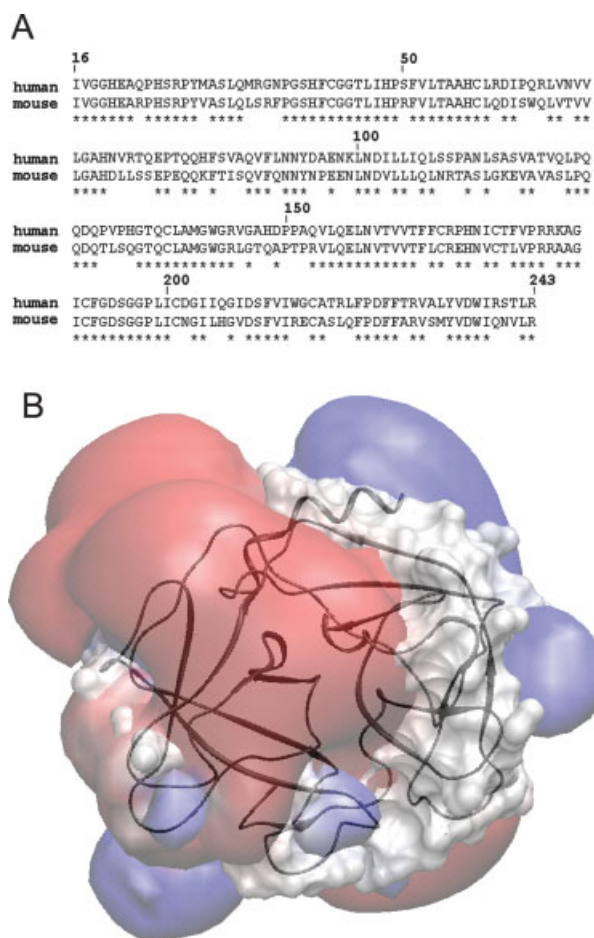


**Figure 8**

The mouse form of proteinase 3. Sequence alignment with human PR3 (A) and electrostatic potential (B) (cf. Fig. 3 for legend). [Color figure can be viewed in the online issue, which is available at [www.interscience.wiley.com](http://www.interscience.wiley.com).]

determinants of the binding of PR3 and HNE to anionic and neutral membranes.

The sequence of mature PR3 does not contain any potential post-translational modification site (S-acylation, myristoylation, prenylation or GPI-linkage). However a careful examination of the sequence (Fig. 2) and structure (Fig. 3) of PR3 led us to identify a putative IBS for PR3; a HC (F165, F166, I217, W218, L223, and F224) sits in the middle of a substantial electropositive region <sup>177</sup>RPHNICTFVPRRK<sup>187</sup> containing a BC.

MD simulations show that PR3 favorably binds to charged or neutral membrane models; the average binding energies are  $-10.87$ ,  $-9.04$ , and  $-3.07$  kcal/mol for the selected simulations with 100%, 50%, and 0% anionic membranes, respectively (Table I). The fact that the binding energies increase with the charge of the membrane supports the idea of a strong electrostatic interaction between a BC and the anionic membrane. We indeed observe that the most favorable contribution to the binding energy is the Gouy–Chapman term (in the case of the anionic membranes), which describes the interaction of the protein with the charged lipid head groups. As described by Murray and col., association of peripheral proteins to membranes is partly mediated by electrostatic interactions<sup>29,64</sup>; nonspecific electrostatic interactions attract and orient the protein to the membrane surface so that hydrophobic motifs (post-translational modifications or conserved amino acids) can insert. The second most important favorable contribution to our calculated binding energy is the change in solvation energy of the hydrophobic and aliphatic groups. Our MD simulations with charged membranes (50% and 100% anionic) thus reproduce this mechanism.

Regardless of the initial orientation, the final configurations of PR3 are very similar, with a value of  $\Theta_{\text{end}}$  between  $8.5^\circ$  and  $40.8^\circ$  (Table I). In the case of the neutral membrane, if the simulation is initiated with the right orientation, PR3 is also found to stably bind the membrane. The three membrane types (Fig. 5) lead to similar conformations and comparable insertion. The IBS corresponds to the region predicted by the analysis of the sequence and structure of PR3. More precisely, several basic residues are found to be close to the membrane upper plane (R177, R186, R186B, K187, R222) while hydrophobic and polar residues (H132, F165, F166, F184, W218, T221, L223, F224) partition into the membranes or remain at the hydrophobic–hydrophilic interface depending on the anionic content. The hydrophobic amino acids correspond to the ones mentioned by Goldmann *et al.* as potential candidates for the anchorage of PR3 to liposomes. The energetic importance of L223, F166, F165, F224, F184, and W218 (50% anionic and zwitterionic) is revealed by their favorable contribution to  $\Delta\Delta G_{\text{solv}}$  ( $\Delta W_{\text{aliphatic}}$ ,  $\Delta W_{\text{aromatic}}$ , and  $\Delta W_{\text{polar}}$ ; Fig. 6). The largest contributions are found for F166 and L223 with  $-1.5$  and  $-2.2$  kcal/mol, respectively, at the 100%

anionic membranes. To confirm the importance of these amino acids, we repeated the simulations starting with orientation 6 for both the zwitterionic and 50% anionic membranes, with a variant of PR3 where both L223 and F166 are replaced by alanines. The simulations were performed for both the 50% anionic and zwitterionic membranes. The interfacial insertion of the mutated PR3 is completely disrupted; the protein moves away from both the charged and neutral membrane plane. In the case of anionic membranes, there is a residual binding energy which only reflects the long-range electrostatic interactions of charged residues of PR3 with the negatively charged membrane.

Our results suggest that PR3 can bind stably to anionic and neutral membranes, with a stronger binding to negatively charged bilayers. We also demonstrate that it has a unique and well-defined IBS. We show that only a few residues of PR3 account for the membrane anchorage. The interaction between the basic residues (BC) at the surface of PR3 and the membrane provides the driving force to orient PR3 at the membrane surface, so that the hydrophobic residues (HC) can anchor into the nonpolar region of the membrane. The hydrophobic residues indeed act as a binding motif with a high affinity for the membrane.

It is clear nowadays that electrostatic interactions are often not enough to explain interfacial binding.<sup>31</sup> For secreted phospholipases A2 the role of hydrophobic residues has been shown to support interfacial binding; specifically the importance of tryptophanes has been demonstrated for several members of the family.<sup>65</sup> In a study using fluorescence techniques, a short hydrophobic loop of the toxin perfringolysin O (PFO) is found to insert in the membrane core; this is the mechanism by which PFO anchors before undergoing major structural rearrangements and form a membrane pore.<sup>66</sup>

The mechanism we describe (electrostatically driven attraction thanks to BC and insertion of HC) is not incompatible with the presence of a partner protein.<sup>11,13,67</sup> Such interactions might simply reinforce or perpetuate the membrane anchorage and/or facilitate the function(s) of mPR3.

Goldmann *et al.* reported that PR3 binds to anionic and zwitterionic reconstituted liposomes.<sup>15</sup> This remarkably agrees with our findings. They also show that the liposome-associated PR3 is catalytically active but with  $V_{\text{max}}$  and  $K_{\text{m}}$  values two-fold lower than the free enzyme. Another study shows that mPR3 is catalytically active against various peptidic substrates; however, mPR3 would only be partially inhibited by a high molecular mass inhibitor such as  $\alpha 1$ -PI.<sup>9</sup> Our calculations show that in the final orientation of PR3 to model membranes its active site is still accessible. To visually evaluate the steric hindrance caused by the presence of the membrane on the substrate binding sites of PR3, we manually docked a heptapeptide (AAPVKGD) and  $\alpha 1$ -PI in mPR3 (proce-

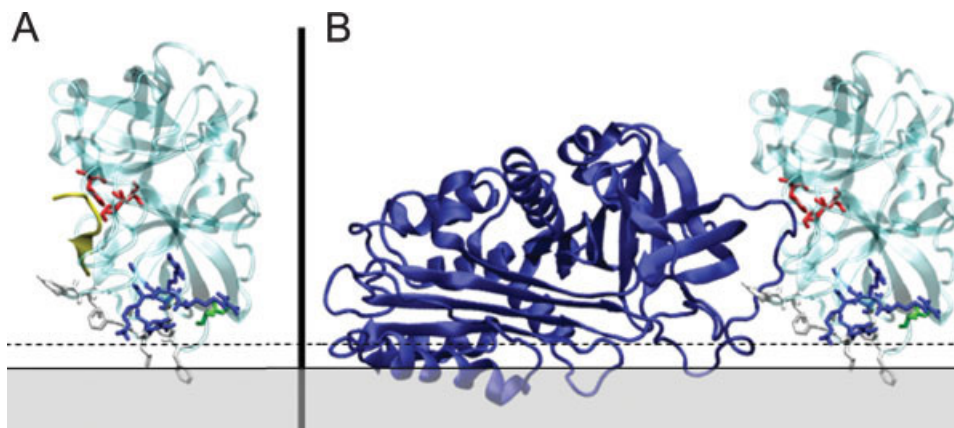


**Figure 9**

Accessibility of mPR3 binding site to (A) a heptapeptide and (B)  $\alpha 1$ -PI. (cf. legend of Fig. 5). The catalytic triad of Pr3 is displayed in licorice and colored in red. (A) The heptapeptide AAPVKGD is colored in yellow. (B). The secondary structure of the 376-residue long  $\alpha 1$ -proteinase inhibitor ( $\alpha 1$ -PI) is colored in dark blue. [Color figure can be viewed in the online issue, which is available at [www.interscience.wiley.com](http://www.interscience.wiley.com).]

ture as reported in Ref. 61). Figure 9(A) shows that the peptide does not encounter steric hindrance with the membrane. On the other hand, the inhibitor  $\alpha 1$ -PI “overlaps” with the membrane region [cf. Fig. 9(B)]. This confirms the hypothesis made by Campbell *et al.* that steric hindrance prevents the inhibition of mPR3 by  $\alpha 1$ -PI.

The results of Goldmann *et al.* and ours agree on the fact that PR3 membrane binding is dependent on the lipid composition and is more favorable with negatively charged membranes. Although our simulations show a more favorable binding of PR3 to 100% anionic than to 50% anionic membranes, they report that the binding to 50% anionic is more favorable than for the 100% anionic membranes, with  $K_d$  values of 4.5  $\mu M$  and 14.5  $\mu M$ , respectively. Such a small energy difference (0.7 kcal/mol) is within our error bar ( $\pm 1$  kcal/mol). In addition, implicit membrane models do not account for lipid demixing, lipid packing, or discrete charge effects. Lipid demixing and their effects have been extensively described previously<sup>68,69</sup>; reorganization of charged and neutral lipids around an IBS containing both charged and hydrophobic amino acids would certainly optimize the binding affinity of the protein.

In our simulations, HNE never binds to the zwitterionic membrane regardless of its starting orientations. This is in agreement with Goldmann *et al.*<sup>15</sup> who report that PR3 unlike HNE associates with zwitterionic liposomes. Our calculations show that HNE does not reorient to present a unique IBS to the anionic membranes and only associates with the membrane when the simulations are initiated with orientation 6. Since this is the simulation with the lowest effective energy, we hypothesize that the interacting region of HNE obtained from this simulation is its IBS. It is in the same region of the

protein structure as the one of PR3. Compared to PR3, the IBS of HNE contains less hydrophobic residues and more basic residues (Fig. 7). There are no phenylalanines or tryptophanes near the membrane surface; only two leucines (L166 and L223) are observed to insert into the nonpolar region of the membrane. The only simulation of HNE that leads to an insertion in the membrane (simulation 6) yields lower binding energies in 100% and 50% anionic membranes ( $-18.52$  and  $-12.65$  kcal/mol, respectively) than the ones obtained for PR3 ( $-10.87$  and  $-9.04$ , respectively). This is largely explained by the Gouy–Chapman contribution, which in the case of HNE describes the interaction between the anionic lipids and a highly positively charged protein (net charge +11), in particular with seven arginines (cf. Fig. 7). However, Goldmann *et al.* reported that the affinity of HNE for anionic membranes is lower than that of PR3. On the other hand, Campbell *et al.*<sup>9</sup> showed that PR3 can be eluted from the surface of stimulated PMNs with solutions of lower ionic strength than HNE and CatG, thereby suggesting a stronger ionic interaction to membranes for HNE and CatG than for PR3. Until additional biophysical data are available, it is very difficult to conclude on the relative binding strength of PR3 and HNE. We believe that the electrostatic interactions of HNE with anionic lipids are stronger than those of PR3, but also that PR3 has a more specific IBS than HNE and is more likely to deeply anchor into the membranes and to make strong hydrophobic interactions while the insertion of HNE might be more shallow.

Recent work pointed out the importance of considering the differences between murine and human PR3 for murine model experiments for the development of animal models for anticytoplasmic neutrophil autoantibodies (ANCA)-associated vasculitis.<sup>70</sup> Wiesner *et al.* showed

species-specific physicochemical properties and substrate specificities. In particular, they observe that mouse PR3 is more easily dislodged from its intracellular storage compartments in HMC-1 cells than human PR3 suggesting different interactions with cell surfaces. Comparison between the human and mouse sequences shows that half of the 11 amino acids of the putative IBS of the human form are not conserved in the mouse form. Of importance is the fact that the mouse form lacks three aromatic and one basic amino acid compared to the human form. The former are known, from integral membrane proteins, to be found at the membrane interface while the latter provides electrostatic interactions with the lipid polar heads. In addition, the mouse form is globally more electronegative than the human form [Fig. 8(B)]. This is in agreement with the difference in pI values between the mouse and human enzymes; the calculated (7.7) and experimental pI (9.1<sup>71</sup> or >9.5<sup>72</sup>) of human PR3 are much higher than the calculated value (6.7) of mouse PR3. We believe that mouse PR3 can bind to the plasma membrane using the same region as human PR3 but that it binds less strongly and specifically. This correlates with the observation of Wiesner *et al.*<sup>70</sup> However, additional theoretical and biophysical studies are needed to undoubtedly identify the mouse/rat IBS and its membrane-binding affinity.

PR3 is the main target autoantigen of ANCA, which predominate in patients with Wegener's granulomatosis. There is growing evidence that ANCAs have a pathogenic role in systemic vasculitis, and there is thus an interest in identifying the interacting regions of PR3. Many attempts have been made to characterize the ANCA epitopes on PR3.<sup>73,74</sup> Even though it has been shown in 1992 that they recognize conformational epitopes,<sup>75</sup> many studies used linear peptides to probe ANCA epitopes of PR3.<sup>76–79</sup> Although there is little overlap between the results from these studies, it seems clear that none of the epitopes are located in the signal peptide or C-terminal peptide of PR3 and that some epitopes are located in close proximity of the catalytic triad. Steric hindrance will prevent ANCA from binding to regions of PR3 too close to the membrane. Since ANCA cannot bind membrane PR3 on the same region as it uses to bind to the membrane we would rule out the IBS and the surrounding residues as potential epitopes (such as FCRPHNI<sup>76</sup> or RRKAGI<sup>76,79</sup>). On the other hand, epitopes including the catalytic His and Ser or the surrounding loops seem compatible with the membrane-binding site we predict in this study.

The implicit membrane models IMM1 and IMM1-GC have been successfully used to investigate several membrane proteins and their reliability have been largely assessed.<sup>37,40,41</sup> In addition the quantitative agreement between our calculations and available biophysics measurements confirms the appropriateness of this model for PR3. It allowed us to (i) calculate the binding energies and dissect them to identify the contributions important

for the membrane anchorage, (ii) identify the amino acids constituting the IBS, and (iii) get a dynamic picture of the binding mechanism. The lipid demixing effects and the details of the interactions between various lipids and PR3 cannot be described using IMM1-GC and would have required an explicit description of the membrane. However, such a description is costly in computer resources and would not have allowed us to screen the surface of PR3 to identify the IBS.

We presented here the first study of the structural determinants of the binding of PR3 to anionic and neutral membranes. To our knowledge there exist no experimental data describing the structure of mPR3, nor of its IBS. This is understandable if one considers the challenges posed by the study of peripheral membrane proteins by structural biology techniques such as NMR or X-ray. Theoretical biophysics has proven extremely useful to unravel membrane binding mechanism of peptides and proteins (e.g. see Refs. 24, 26–28, 31, 43, and 80) and is in many cases, until the experimental difficulties are overcome, the method of choice to evaluate the energetics of membrane binding and predict IBSs.

Our work demonstrates that the interaction between PR3 and the plasma membrane is not mediated only by electrostatic interactions but involves the insertion of a large HC in anionic and neutral membranes. This is a unique feature of PR3 not shared by HNE. Taking into account this characteristic feature of PR3 we can foresee that specific functions will be mediated by membrane PR3 which can be externalized during apoptosis in the absence of degranulation.<sup>14,81</sup> Our working hypothesis is that molecular analysis of PR3/membrane association in combination with other partners in neutrophils will help us to unravel the role of PR3 in inflammatory diseases and especially in Wegener's granulomatosis. Our predictions open a new avenue of research but still need to be challenged by biochemical experiments. Hence, our long-term objective is to better understand the molecular mechanisms involved in PR3/membrane interaction in neutrophils. This work constitutes the first step in the rational design of drugs aimed at modulating PR3 membrane expression and at proposing novel anti-inflammatory therapeutic strategies.

## ACKNOWLEDGMENTS

Parallab (High Performance Computing Laboratory at the University of Bergen) is thankfully acknowledged for provision of CPU time on its supercomputers. Anna-Mulgrew Nesbitt and Knut Børve are thanked for fruitful discussions.

## REFERENCES

1. Witko-Sarsat V, Rieu P, Descamps-Latscha B, Lesavre P, Halbwachs-Mecarelli L. Neutrophils: molecules, functions and pathophysiological aspects. *Lab Invest* 2000;80:617–653.

2. Nathan C. Neutrophils and immunity: challenges and opportunities. *Nat Rev Immunol* 2006;6:173–182.
3. Owen CA, Campbell EJ. The cell biology of leukocyte-mediated proteolysis. *J Leukoc Biol* 1999;65:137–150.
4. Campbell EJ, Campbell MA, Boukedes SS, Owen CA. Quantum proteolysis by neutrophils: implications for pulmonary emphysema in  $\alpha$ 1-antitrypsin deficiency. *J Clin Invest* 1999;104:337–344.
5. Witko-Sarsat V, Lesavre P, Lopez S, Bessou G, Hieblot C, Prum B, Noel LH, Guillevin L, Ravaud P, Sermet-Gaudelus I, Timsit J, Grunfeld JP, Halbwachs-Mecarelli L. A large subset of neutrophils expressing membrane proteinase 3 is a risk factor for vasculitis and rheumatoid arthritis. *J Am Soc Nephrol* 1999;10:1224–1233.
6. Witko-Sarsat V, Cramer EM, Hieblot C, Guichard J, Nusbaum P, Lopez S, Lesavre P, Halbwachs-Mecarelli L. Presence of proteinase 3 in secretory vesicles: evidence of a novel, highly mobilizable intracellular pool distinct from azurophilic granules. *Blood* 1999;94:2487–2496.
7. Rarok AA, Stegeman CA, Limburg PC, Kallenberg CG. Neutrophil membrane expression of proteinase 3 (PR3) is related to relapse in PR3-ANCA-associated vasculitis. *J Am Soc Nephrol* 2002;13:2232–2238.
8. Schreiber A, Busjahn A, Luft FC, Kettritz R. Membrane expression of proteinase 3 is genetically determined. *J Am Soc Nephrol* 2003;14:68–75.
9. Campbell EJ, Campbell MA, Owen CA. Bioactive proteinase 3 on the cell surface of human neutrophils: quantification, catalytic activity, and susceptibility to inhibition. *J Immunol* 2000;165:3366–3374.
10. David A, Fridlich R, Aviram I. The presence of membrane proteinase 3 in neutrophil lipid rafts and its colocalization with Fc $\gamma$ RIIIb and cytochrome b558. *Exp Cell Res* 2005;308:156–165.
11. Fridlich R, David A, Aviram I. Membrane proteinase 3 and its interactions within microdomains of neutrophil membranes. *J Cell Biochem* 2006;99:117–125.
12. Bauer S, Abdgawad M, Gunnarsson L, Segelmark M, Tapper H, Hellmark T. Proteinase 3 and CD177 are expressed on the plasma membrane of the same subset of neutrophils. *J Leukoc Biol* 2007;81:458–464.
13. von Vietinghoff S, Tunnemann G, Eulenberg C, Wellner M, Cardoso MC, Luft FC, Kettritz R. NB1 mediates surface expression of the ANCA antigen proteinase 3 on human neutrophils. *Blood* 2007;109:4487–4493.
14. Kantari C, Pederzoli-Ribeil M, Amir-Moazami O, Gausson-Dorey V, Moura IC, Lecomte MC, Benhamou M, Witko-Sarsat V. Proteinase 3, the Wegener autoantigen, is externalized during neutrophil apoptosis: evidence for a functional association with phospholipid scramblase 1 and interference with macrophage phagocytosis. *Blood*, in press.
15. Goldmann WH, Niles JL, Arnaout MA. Interaction of purified human proteinase 3 (PR3) with reconstituted lipid bilayers. *Eur J Biochem* 1999;261:155–162.
16. Fujinaga M, Cherniaia MM, Halenbeck R, Kothe K, James MN. The crystal structure of PR3, a neutrophil serine proteinase antigen of Wegener's granulomatosis antibodies. *J Mol Biol* 1996;261:267–278.
17. Capener CE, Kim HJ, Arinaminpathy Y, Sansom MS. Ion channels: structural bioinformatics and modelling. *Hum Mol Genet* 2002;11:2425–2433.
18. Roux B, Allen T, Berneche S, Im W. Theoretical and computational models of biological ion channels. *Q Rev Biophys* 2004;37:15–103.
19. Roux B, Schulten K. Computational studies of membrane channels. *Structure* 2004;12:1343–1351.
20. Tieleman DP. Computer simulations of transport through membranes: passive diffusion, pores, channels and transporters. *Clin Exp Pharmacol Physiol* 2006;33:893–903.
21. Noskov SY, Roux B. Ion selectivity in potassium channels. *Biophys Chem* 2006;124:279–291.
22. Stahelin RV, Ananthanarayanan B, Blatner NR, Singh S, Bruzik KS, Murray D, Cho W. Mechanism of membrane binding of the phospholipase D1 PX domain. *J Biol Chem* 2004;279:54918–54926.
23. McLaughlin S, Murray D. Plasma membrane phosphoinositide organization by protein electrostatics. *Nature* 2005;438:605–611.
24. Dalton AK, Murray PS, Murray D, Vogt VM. Biochemical characterization of rous sarcoma virus MA protein interaction with membranes. *J Virol* 2005;79:6227–6238.
25. Wijewickrama GT, Albanese A, Kim YJ, Oh YS, Murray PS, Takayanagi R, Tobe T, Masuda S, Murakami M, Kudo I, Ucker DS, Murray D, Cho W. Unique membrane interaction mode of group IIF phospholipase A2. *J Biol Chem* 2006;281:32741–32754.
26. Sammalkorpi M, Lazaridis T. Modeling a spin-labeled fusion peptide in a membrane: implications for the interpretation of EPR experiments. *Biophys J* 2007;92:10–22.
27. Sammalkorpi M, Lazaridis T. Configuration of influenza hemagglutinin fusion peptide monomers and oligomers in membranes. *Biochim Biophys Acta* 2007;1768:30–38.
28. Jaud SE. Self-induced docking site of a deeply embedded peripheral membrane protein. *Biophys J* 2007;92:517–524.
29. Diraviyam K, Stahelin RV, Cho W, Murray D. Computer modeling of the membrane interaction of FYVE domains. *J Mol Biol* 2003;328:721–736.
30. Stahelin RV, Long F, Diraviyam K, Bruzik KS, Murray D, Cho W. Phosphatidylinositol 3-phosphate induces the membrane penetration of the FYVE domains of Vps27p and Hrs. *J Biol Chem* 2002;277:26379–26388.
31. Mulgrew-Nesbitt A, Diraviyam K, Wang J, Singh S, Murray P, Li Z, Rogers L, Mirkovic N, Murray D. The role of electrostatics in protein–membrane interactions. *Biochim Biophys Acta* 2006;1761:812–826.
32. Arbuza A, Wang L, Wang J, Hangyas-Mihalyne G, Murray D, Honig B, McLaughlin S. Membrane binding of peptides containing both basic and aromatic residues. Experimental studies with peptides corresponding to the scaffolding region of caveolin and the effector region of MARCKS. *Biochemistry* 2000;39:10330–10339.
33. Murray D, Hermida-Matsumoto L, Buser CA, Tsang J, Sigal CT, Ben-Tal N, Honig B, Resh MD, McLaughlin S. Electrostatics and the membrane association of Src: theory and experiment. *Biochemistry* 1998;37:2145–2159.
34. Murray D, Honig B. Electrostatic control of the membrane targeting of C2 domains. *Mol Cell* 2002;9:145–154.
35. Dumas JJ, Merithew E, Sudharshan E, Rajamani D, Hayes S, Lawe D, Corvera S, Lambright DG. Multivalent endosome targeting by homodimeric EEA1. *Mol Cell* 2001;8:947–958.
36. Grossfield A, Feller SE, Pitman MC. Convergence of molecular dynamics simulations of membrane proteins. *Proteins* 2007;67:31–40.
37. Lazaridis T. Effective energy function for proteins in lipid membranes. *Proteins* 2003;52:176–192.
38. Im W, Feig M, Brooks CL. An implicit membrane generalized born theory for the study of structure, stability, and interactions of membrane proteins. *Biophys J* 2003;85:2900–2918.
39. Feig M, Brooks CL, III. Recent advances in the development and application of implicit solvent models in biomolecule simulations. *Curr Opin Struct Biol* 2004;14:217–224.
40. Lazaridis T. Implicit solvent simulations of peptide interactions with anionic lipid membranes. *Proteins* 2005;58:518–527.
41. Mihajlovic M, Lazaridis T. Calculations of pH-dependent binding of proteins to biological membranes. *J Phys Chem B* 2006;110:3375–3384.
42. Zhang J, Lazaridis T. Calculating the free energy of association of transmembrane helices. *Biophys J* 2006;91:1710–1723.
43. Mihajlovic M, Lazaridis T. Membrane-bound structure and energetics of  $\alpha$ -synuclein. *Proteins: Struct Funct Bioinf*, in press.
44. Mihajlovic M, Lazaridis T. Modeling fatty acid delivery from intestinal fatty acid binding protein to a membrane. *Protein Sci* 2007;16:2042–2055.

45. Magee T, Seabra MC. Fatty acylation and prenylation of proteins: what's hot in fat. *Curr Opin Cell Biol* 2005;17:190–196.
46. Linder ME, Deschenes RJ. Palmitoylation: policing protein stability and traffic. *Nat Rev Mol Cell Biol* 2007;8:74–84.
47. Resh MD. Fatty acylation of proteins: new insights into membrane targeting of myristoylated and palmitoylated proteins. *Biochim Biophys Acta* 1999;1451:1–16.
48. Glomset JA, Gelb MH, Farnsworth CC. Prenyl proteins in eukaryotic cells: a new type of membrane anchor. *Trends Biochem Sci* 1990;15:139–142.
49. Glomset JA, Gelb MH, Farnsworth CC. Geranylgeranylated proteins. *Biochem Soc Trans* 1992;20:479–484.
50. Sinensky M, Lutz RJ. The prenylation of proteins. *Bioessays* 1992;14:25–31.
51. Eisenhaber B, Bork P, Eisenhaber F. Prediction of potential GPI-modification sites in proprotein sequences. *J Mol Biol* 1999;292:741–758.
52. Eisenhaber B, Bork P, Eisenhaber F. Sequence properties of GPI-anchored proteins near the omega-site: constraints for the polypeptide binding site of the putative transamidase. *Protein Eng* 1998;11:1155–1161.
53. Sunyaev SR, Eisenhaber F, Rodchenkov IV, Eisenhaber B, Tumanyan VG, Kuznetsov EN. PSIC: profile extraction from sequence alignments with position-specific counts of independent observations. *Protein Eng* 1999;12:387–394.
54. Eisenhaber B, Bork P, Yuan Y, Löffler G, Eisenhaber F. Automated annotation of GPI anchor sites: case study *C. elegans*. *Trends Biochem Sci* 2000;25:340–341.
55. Nicholls A, Sharp KA, Honig B. Protein folding and association: insights from the interfacial and thermodynamic properties of hydrocarbons. *Proteins* 1991;11:281–296.
56. Humphrey W, Dalke A, Schulten K. VMD—visual molecular dynamics. *J Mol Graphics* 1996;14:33–38.
57. Neria E, Fischer S, Karplus M. Simulation of activation free energies in molecular systems. *J Chem Phys* 1996;105:1902–1921.
58. Mclaughlin S. The electrostatic properties of membranes. *Annu Rev Biophys Chem* 1989;18:113–136.
59. Brooks BR, Brucoleri RE, Olafson BD, States DJ, Swaminathan S, Karplus M. CHARMM: a program for macromolecular energy. Minimization, and dynamics calculations *J Comput Chem* 1983;4:187–217.
60. Bode W, Wei A, Huber R, Meyer E, Travis J, Neumann S. X-ray crystal structure of the complex of human leukocyte elastase (PMN elastase) and the third domain of the turkey ovomucoid inhibitor. *EMBO J* 1986;5:2453–2458.
61. Hajjar E, Korkmaz B, Gauthier F, Brandsdal BO, Witko-Sarsat V, Reuter N. Inspection of the binding sites of proteinase 3 for the design of a highly specific substrate. *J Med Chem* 2006;49:1248–1260.
62. Brunger AT, Karplus M. Polar hydrogen positions in proteins: empirical energy placement and neutron diffraction comparison. *Proteins* 1988;4:148–156.
63. Sali A, Blundell TL. Comparative protein modelling by satisfaction of spatial restraints. *J Mol Biol* 1993;234:779–815.
64. Diraviyam K, Murray D. Computational analysis of the membrane association of group IIA secreted phospholipases A2: a differential role for electrostatics. *Biochemistry* 2006;45:2584–2598.
65. Gelb MH, Cho WH, Wilton DC. Interfacial binding of secreted phospholipases A(2): more than electrostatics and a major pole for tryptophan. *Curr Opin Struct Biol* 1999;9:428–432.
66. Ramachandran R, Heuck AP, Tweten RK, Johnson AE. Structural insights into the membrane-anchoring mechanism of a cholesterol-dependent cytolysin. *Nat Struct Biol* 2002;9:823–827.
67. Gabay JE, Scott RW, Campanelli D, Griffith J, Wilde C, Marra MN, Seeger M, Nathan CF. Antibiotic proteins of human polymorphonuclear leukocytes. *Proc Natl Acad Sci USA* 1989;86:5610–5614.
68. Kasbauer M, Bayerl TM. Formation of domains of cationic or anionic lipids in binary lipid mixtures increases the electrostatic coupling strength of water-soluble proteins to supported bilayers. *Biochemistry* 1999;38:15258–15263.
69. Laura LM, Coutinho A, Silva A, Fedorov A, Prieto M. Structural effects of a basic peptide on the organization of dipalmitoylphosphatidylcholine/dipalmitoylphosphatidylserine membranes: a fluorescent resonance energy transfer study. *J Phys Chem B* 2006;110:8130–8141.
70. Wiesner O, Litwiller RD, Hummel AM, Viss MA, McDonald CJ, Jenne DE, Fass DN, Specks U. Differences between human proteinase 3 and neutrophil elastase and their murine homologues are relevant for murine model experiments. *FEBS Lett* 2005;579:5305–5312.
71. Kao RC, Wehner NG, Skubitz KM, Gray BH, Hoidal JR. Proteinase 3. A distinct human polymorphonuclear leukocyte proteinase that produces emphysema in hamsters. *J Clin Invest* 1988;82:1963–1973.
72. Campanelli D, Detmers PA, Nathan CF, Gabay JE. Azurocidin and a homologous serine protease from neutrophils. Differential antimicrobial and proteolytic properties. *J Clin Invest* 1990;85:904–915.
73. van der Geld YM, Stegeman CA, Kallenberg CG. B cell epitope specificity in ANCA-associated vasculitis: does it matter? *Clin Exp Immunol* 2004;137:451–459.
74. Muller A, Voswinkel J, Gottschlich S, Csernok E. Human proteinase 3 (PR3) and its binding molecules: implications for inflammatory and PR3-related autoimmune responses. *Ann NY Acad Sci* 2007;1109:84–92.
75. Bini P, Gabay JE, Teitel A, Melchior M, Zhou JL, Elkon KB. Antineutrophil cytoplasmic autoantibodies in Wegener's granulomatosis recognize conformational epitope (s) on proteinase 3. *J Immunol* 1992;149:1409–1415.
76. Williams RC, Jr, Staud R, Malone CC, Payabyab J, Byres L, Underwood D. Epitopes on proteinase-3 recognized by antibodies from patients with Wegener's granulomatosis. *J Immunol* 1994;152:4722–4737.
77. Chang L, Binos S, Savage J. Epitope mapping of anti-proteinase 3 and anti-myeloperoxidase antibodies. *Clin Exp Immunol* 1995;102:112–119.
78. Griffith ME, Coulthart A, Pemberton S, George AJ, Pusey CD. Anti-neutrophil cytoplasmic antibodies (ANCA) from patients with systemic vasculitis recognize restricted epitopes of proteinase 3 involving the catalytic site. *Clin Exp Immunol* 2001;123:170–177.
79. Van Der Geld YM, Simpelaar A, Van Der Zee R, Tervaert JW, Stegeman CA, Limburg PC, Kallenberg CG. Antineutrophil cytoplasmic antibodies to proteinase 3 in Wegener's granulomatosis: epitope analysis using synthetic peptides. *Kidney Int* 2001;59:147–159.
80. Dalton AK, Ako-Adjei D, Murray PS, Murray D, Vogt VM. Electrostatic interactions drive membrane association of the HIV-1 Gag MA domain. *J Virol* 2007;81:6434–6445.
81. Durant S, Pederzoli M, Lepelletier Y, Canteloup S, Nusbaum P, Lesavre P, Witko-Sarsat V. Apoptosis-induced proteinase 3 membrane expression is independent from degranulation. *J Leukoc Biol* 2004;75:87–98.